

Input Sequence and Parameter Estimation in Impulsive Biomedical Models*

Håkan Runvik¹ and Alexander Medvedev¹

Abstract—A hybrid model for biomedical time series comprising a continuous second-order linear time-invariant system driven by an input sequence of positively weighted Dirac delta-functions is considered. The problem of the joint estimation of the input sequence and the continuous system parameters from output measurements is investigated. A solution that builds upon and refines a previously published least-squares formulation is proposed. Based on a thorough analysis of the properties of the least-squares solution, improvements in terms of accuracy and ease of use are achieved on synthetic data, compared to the original algorithm.

I. INTRODUCTION

Signals exhibiting slow, dissipative dynamics that are interrupted by multiple rapid bursts occur in many biological systems. Common examples are found in e.g. endocrinology, since pulsatility is recognized as a fundamental property in the secretion of most hormones [1]. In pharmacokinetics, multi-peaking phenomena in drug concentration [2] can also display such characteristics. There is no generally accepted approach to mathematical modeling of these behaviors. In the endocrine case, a popular construct features a linear plant to portray the hormone elimination fed with an input signal that represents the secretion episodes. For instance, a Gaussian input signal shape is assumed in [3], which enables deconvolution-based input estimation.

To avoid additional assumptions, a pulsatile time series is modeled by a linear plant with impulsive input in this work. In closed loop, this setup was developed for modeling testosterone regulation in [4], while a similar model was employed for pharmacokinetic applications in [5]. The estimation of the input sequence and continuous plant parameters is treated. Least-squares (LS) methods were previously used to address this hybrid identification problem [6], [7], while a Laguerre domain approach was employed for the input estimation in [8]. The present work is based on the same optimization formulation as [7], where LASSO (least absolute shrinkage and selection operator) regularization was used. Yet, a more rigorous estimation procedure is achieved based on a comprehensive analysis of the underlying optimization problem. The main contribution is in the optimization problem analysis that underpins the theoretical foundation of the identification approach. Further, the resulting estimation method does not

*This work is funded in part by the PhD program at the Centre for Interdisciplinary Mathematics, Uppsala University, Sweden and the Swedish Research Council Grant 2019-04451 for the project “Synchronization and entrainment in the impulsive Goodwin’s oscillator”.

¹H. Runvik and A. Medvedev are with the department of Information Technology, Uppsala University, Uppsala, Sweden, {hakan.runvik, alexander.medvedev}@it.uu.se

require user-defined data-dependent parameters and displays better performance as well as ease of implementation.

The rest of the paper is organized as follows. First, the model and estimation problem are formulated. Then, an analysis of the parameter-dependent characteristics of the LS solution is performed and shown to enable an efficient estimation of the parameters in the noise-free case. Finally, the method is generalized to account for noise and uncertainties and experimental results for synthetic data are presented.

II. ESTIMATION PROBLEM

A. Model description

Consider the impulsive sequence

$$\xi(t) = \sum_{k=0}^{\infty} d_k \delta(t - \tau_k), \quad (1)$$

where $\delta(\cdot)$ is the Dirac delta function and d_k and τ_k determine the positive impulse weights and times. It is fed into a linear time-invariant compartmental state-space model

$$\dot{x} = Ax + B\xi(t), \quad y = Cx, \quad x = [x_1 \quad x_2]^T, \quad (2)$$

where

$$A = \begin{bmatrix} -b_1 & 0 \\ g_1 & -b_2 \end{bmatrix}, \quad B = \begin{bmatrix} 1 \\ 0 \end{bmatrix}, \quad C = \begin{bmatrix} 0 \\ 1 \end{bmatrix}^T, \quad (3)$$

with positive parameters b_1, b_2, g_1 . Defining the Heaviside step function as $H(t)$ and assuming the initial state $x(t_0) = x_0$, the output of the system can in a straightforward manner be calculated as

$$\begin{aligned} y(t) &= C \left(e^{A(t-t_0)} x_0 + \int_{t_0}^t e^{A(t-\tau)} B \xi(\tau) d\tau \right) \\ &= C e^{A(t-t_0)} x_0 + \sum_{k=0}^{\infty} g_1 d_k z(b_1, b_2, t - \tau_k), \end{aligned}$$

where

$$z(b_1, b_2, t) = \frac{e^{-b_2 t} - e^{-b_1 t}}{b_1 - b_2} H(t).$$

B. Estimation problem formulation

Let the output of (2) be sampled, possibly irregularly, over a finite horizon and result in the measurements $y(t_k)$, where $k = 1, \dots, K$ and $t_k < t_{k+1}$, thus yielding the vector

$$Y = [y(t_1) \quad \dots \quad y(t_K)]^T.$$

Since an impulse in between two sampling times cannot be distinguished in the sampled output from a pair of impulses that occur at the sampling times [7], the impulses are without

loss of generality restricted to occur at the sampling times. Then it holds that

$$Y = \Phi(b_1, b_2)\theta, \quad (4)$$

where

$$\Phi(b_1, b_2) = [\varphi(b_1, b_2, t_1) \quad \dots \quad \varphi(b_1, b_2, t_K)]^\top,$$

$$\varphi(b_1, b_2, t_i) = \begin{bmatrix} e^{-b_2(t_i-t_1)} \\ z(b_1, b_2, t_i - t_1) \\ \vdots \\ z(b_1, b_2, t_i - t_K) \end{bmatrix},$$

$$\theta = [x_2(t_1) \quad d_1 \quad \dots \quad d_{K-1}]^\top.$$

Notice that $\Phi(b_1, b_2)$ is square and that the state $x_2(t_1)$ is included in the formulation rather than x_0 , since $x_2(t_1)$ and d_1 uniquely determine the state of the system for $t > t_1$.

Further, the combined impulse and parameter estimation in system (2) is treated, i.e. the parameters $d_k, k = 1, \dots, K$ and $b_i, i = 1, 2$ are sought. Notice that $g_1 = 1$ can be assumed, as changing this parameter corresponds to scaling of the impulses. Furthermore, assume that $b_1 < b_2$.

An LS optimization formulation introduced in [7] is employed to the problem in hand. In the estimation, $b_i^*, i = 1, 2$ denote the true parameter values while b_i represent the parameters in the LS formulation

$$\hat{\theta}(b_1, b_2) = \arg \min_{\theta} \|Y - \Phi(b_1, b_2)\theta\|^2, \quad (5)$$

where $\|\cdot\|$ is the Euclidean vector norm. The parameter-dependent objective function makes the setup resemble a multi-parametric programming problem (see e.g. [9]). We also use the notation d_k^* for the true impulse weights while d_k represent their estimates for given parameter values b_1 and b_2 (we suppress the dependency for ease of notation).

In the noise-free case, the optimization formulation is unconstrained. The estimate of θ can therefore be calculated via a matrix inversion (the invertibility of Φ is shown in [7]). In the presence of noise or uncertainties, the impulse weights are restricted to be non-negative, which results in a constrained LS problem.

C. Estimation principle

In the noise-free case, the estimation is based on the following properties of the optimization problem in (5), which are given in Proposition 1.

- If $b_1 + b_2 > b_1^* + b_2^*$ and $b_1 > b_1^*$, all impulse estimates solving (5) have positive weights;
- If $b_1 + b_2 < b_1^* + b_2^*$ and $b_1 < b_1^*$, all impulse estimates solving (5) that do not correspond to true impulses have negative weight.

The properties above give rise to the division of the parameter space depicted in the left subplot of Fig. 1. The idea is to utilize the structure of this space to identify b_1^* and b_2^* . A problem arises in the regions marked as unknown, where the signs of the impulse weights solving the optimization

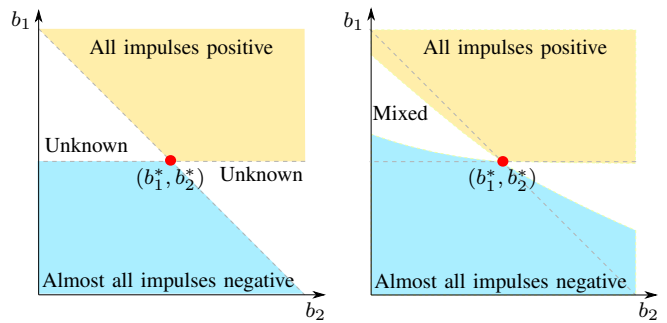


Fig. 1. The division of the b_1 - b_2 parameter space, relative to the true parameter values (b_1^*, b_2^*) , in terms of the solutions to (5). Left: regions with guaranteed signs of impulse weights. Right: region boundaries according to the analysis in Section III-A and numerical experiments. “Mixed” indicates that both positive and negative impulses are present.

problem vary depending on the data. However, theoretical reasoning regarding simplified cases (see Section III-A) indicates that the parameter space will be divided qualitatively according to the right subplot of Fig. 1. This is also observed in numerical experiments. The quantitative behavior (i.e. the slopes of the curves) depends on the values of b_1^*, b_2^* and the distribution of impulses and sampling instances. This refined partitioning enables navigation in the parameter space to the point (b_1^*, b_2^*) , as described in Section III-B.

When noise or uncertainties are present, the parameter space is no longer divided in well-defined regions, as impulses of both signs typically appear in most of the parameter space. However, it is still possible to estimate the boundary of the region with positive impulses, which we denote γ_P . If the noise level is low enough, it is also possible to find an approximation of the true parameter values.

III. NOISE-FREE ESTIMATION

We will first show how the b_1 - b_2 parameter space is divided into the regions indicated above. The analysis is based on the following lemma.

Lemma 1: Let $y(t)$ be the response of system (2) to the input $d_1\delta(t - t_1)$ with $x_0 = [0 \quad 0]^\top$. Denote the response of an estimate of (2) with the parameters \hat{b}_1, \hat{b}_2 to the input $\hat{d}_1\delta(t - \hat{t}_1)$ as $\hat{y}(t)$. Assume that $\hat{b}_1 + \hat{b}_2 > b_1 + b_2$, $\hat{b}_1 > b_1$ and $\hat{b}_1 > \hat{b}_2$. Then, there exist at most two $\tau > \max\{t_1, \hat{t}_1\}$ such that $y(\tau) = \hat{y}(\tau)$.

Proof: See Appendix I. ■

Provided that the impulse sequence is sparse (i.e. that the set S below is nonempty), the result above can be used to characterize the properties of the solution to (2) in two cases, where the estimated system is either faster or slower than the true dynamics. These are defined in the following proposition.

Proposition 1: Consider LS problem (5) with the initial condition $x_2(t_1) = 0$. Assume that the noise-free measurements Y are produced by (2) and let $S = \{k \in \{1, \dots, K\} \mid d_k^* = 0\}$. If $b_1 + b_2 > b_1^* + b_2^*$ and $b_1 > b_1^*$, then $d_k > 0$ for $k = 1, \dots, K$. If $b_1 + b_2 < b_1^* + b_2^*$ and $b_1 < b_1^*$, then $d_k < 0$ for $k \in S$.

Proof: See Appendix II. ■

Note that Lemma 1 and Proposition 1 apply only when the initial state is zero, while the optimization formulation in (5) allows a nonzero initial value for x_2 (a nonzero initial x_1 can be represented by an impulse and is thus not included in the estimation). However, since the contribution from the initial state tends to zero exponentially, the proposition is expected to hold in the case of nonzero initial conditions too.

A. Boundaries of the sign-definite impulse regions

The proposition above does not provide information about the region which is marked as unknown in the left subplot of Fig. 1. To gain understanding of the behavior in this region, consider a simplified case of three sampled measurements of the response to a single impulse at time $t = 0$. Denote it as $y^*(t)$ and assume that it is generated by (2) with the parameter values b_1^*, b_2^* . Let $y(t)$ be the response of the same system but with parameters b_1, b_2 . The boundary between solutions with positive and negative impulse weights is then defined by the case when $y(t)$ intersects $y^*(t)$ precisely at the sampling times (i.e. no additional positive or negative impulses are required to explain the behavior). If the curves intersect at the times τ, ν, μ , the relation between b_1, b_2 and b_1^*, b_2^* is given by a solution to the equation

$$(\chi^\tau - \psi^\tau)(\omega^\mu - \omega^\nu) + (\chi^\nu - \psi^\nu)(\omega^\tau - \omega^\mu) + (\chi^\mu - \psi^\mu)(\omega^\nu - \omega^\tau) = 0, \quad (6)$$

where $\chi = e^{b_1 - b_2^*}$, $\psi = e^{b_1 - b_1^*}$ and $\omega = e^{b_1 - b_2}$. Note that equation (6) has $b_1 = b_2$ as another, infeasible solution. By solving (6) for ω , an expression for b_2 would be obtained. However, since solving (6) algebraically for ω is not possible in a general case, only equidistant sampling, i.e. $\nu = \tau + c, \mu = \tau + 2c$, where $c > 0$, is considered. The feasible solution then becomes

$$\begin{aligned} b_2 &= b_1 - \ln(\omega) \\ &= b_1 - \frac{1}{c} \ln \left(\frac{\chi^{\tau+c} - \chi^{\tau+2c} - \psi^{\tau+c} + \psi^{\tau+2c}}{\chi^\tau - \chi^{\tau+c} - \psi^\tau + \psi^{\tau+c}} \right) \\ &\triangleq b_1 - \frac{1}{c} \ln \left(\frac{\omega_1}{\omega_2} \right), \end{aligned}$$

where the solution naturally is $b_2 = b_2^*$ if $b_1 = b_1^*$. Taking the derivative with respect to b_1 yields

$$\frac{db_2}{db_1} = -1 + (\chi^{\tau+c} - \psi^{\tau+c}) \left(\frac{1}{\omega_1} - \frac{1}{\omega_2} \right).$$

Since $b_1 < b_2$, it follows that $\chi < \psi$ and $0 < \omega_1 < \omega_2$. That leads to the inequality

$$-\infty < \frac{db_2}{db_1} < -1.$$

The second derivative, given by

$$\begin{aligned} \frac{d^2 b_2}{db_1^2} &= c(\chi^{\tau+c} - \psi^{\tau+c}) \\ &\times \left(-\frac{1}{\omega_1} - \frac{1}{\omega_2} + (\chi^{\tau+c} - \psi^{\tau+c}) \left(\frac{1}{\omega_1^2} - \frac{1}{\omega_2^2} \right) \right) > 0, \end{aligned}$$

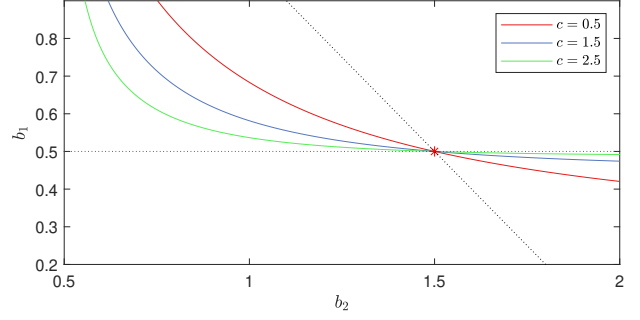


Fig. 2. The pairs of estimates b_1, b_2 resulting in intersections between $y(t)$ and $y^*(t)$ at times $1, 1+c, 1+2c$ for different values of c and $b_1^* = 0.5, b_2^* = 1.5$. The dotted lines represent the theoretical limits for the borders given in Proposition 1.

shows that the derivative changes monotonously. Finally, if the samples are shifted in time relative to the impulse, b_2 changes according to

$$\frac{db_2}{d\tau} = \frac{1}{c} (b_1 - b_2) \psi^{\tau+c} (1 - \psi^c) \left(\frac{1}{\omega_2} - \frac{1}{\omega_1} \right).$$

If $b_1 < b_1^*$, then $\psi < 1$, which makes the expression positive, while $b_1 > b_1^*$ makes it negative, i.e. a shift in time causes a pivot of the curve around the point (b_1^*, b_2^*) . The resulting curves are illustrated in Fig. 2.

If more than three measurements are considered, each triplet of measurements generates a separate b_2 -boundary. For a non-equidistant triplet, the qualitative behavior of the corresponding solution to (6) appears to be similar to that of the equidistant case in numerical experiments. Since a solution with only positive impulses requires that parameter estimates are above all these boundaries, the limiting case, which defines the curve γ_P , corresponds to the largest value of b_2 for a given b_1 . For solutions with almost all impulses being negative, the converse holds. Adding more impulses does not alter this behavior. As all boundaries intersect at $b_1 = b_1^*, b_2 = b_2^*$, and triplets with different time shifts produce different slopes according to the above discussion, this explains the non-smoothness of the boundaries at this point illustrated in Fig. 1. Note that the presented analysis only is valid if the impulses are sufficiently sparse, i.e. there are instances with at least three sampling times in between two impulses.

B. Estimation algorithm

The following procedure is suggested to solve the estimation problem in the absence of noise. Let $d(c)$ denote the distance between the pair of points where the boundaries of the positive and negative impulse regions (see Fig. 1) intersect with the line $b_1 = 2b_2 + c$. Since the boundaries meet at the point (b_1^*, b_2^*) , minimization of $d(c)$ with respect to c recovers the values of b_1^* and b_2^* . The points of intersection which determine $d(c)$ can be calculated with the bisection method, by considering the signs of the estimated impulse weights obtained from solving (5) at points along the line

$b_1 = 2b_2 + c$. Once b_1^* and b_2^* are calculated, Algorithm 1 in [7] is used to calculate the impulse times and weights.

No further details on this algorithm are provided, as only estimation under uncertainties is relevant in applications.

IV. ESTIMATION UNDER UNCERTAINTY

A. Estimation of b_1 and b_2

To represent noise or model uncertainty, we consider the modification of (4)

$$Y = \Phi(b_1, b_2)\theta + \epsilon,$$

where ϵ is a zero-mean noise vector. The parameter space is then no longer divided as in Fig. 1, since the region of mixed impulse weights then covers a larger area and, in particular, includes (b_1^*, b_2^*) . A non-negativity constraint for the impulse weights is for this reason added to (5). In the absence of noise, this would leave the region above γ_P unaffected, while rendering the residual sum of squares

$$\|Y - \Phi(b_1, b_2)\hat{\theta}(b_1, b_2)\|^2 \triangleq g(b_1, b_2) \quad (7)$$

nonzero in the rest of the parameter space. In particular, for a fixed value $b_2 = \bar{b}_2$ such that (\bar{b}_1, \bar{b}_2) is on γ_P , $g(b_1, \bar{b}_2)$ is expected to be decreasing in b_1 when $b_1 < \bar{b}_1$. In the noisy setting, the qualitative behavior tends to be similar, but the residual sum is nonzero even for $b_1 > \bar{b}_1$. We will utilize this property to estimate γ_P using the following result.

Lemma 2: Let $f(x) = c_1(x - x^*)^2 + c_2$, where $c_1, c_2 > 0$. Define $N_f(x)$ and \hat{x} by

$$N_f(x) = -\frac{f(x)}{df(x)/dx},$$

$$\hat{x} = \arg \min_x N_f(x) + \min_x N_f(x),$$

$$\text{s.t. } \min_x N_f(x) > 0.$$

Then $\hat{x} = x^*$.

Proof: Straightforward minimization. ■

The minimization problem stated in the lemma is applied to the residual sum of squares $g(b_1, \bar{b}_2)$, i.e. the function is assumed to be approximately quadratic, somewhat similarly to Newton's method in optimization. The point of this technique is that the objective function only is required to be quadratic below γ_P , so the optimization can be performed even though $g(b_1, \bar{b}_2)$ does not have a unique minimum close to γ_P .

Generalizing to incorporate both b_1 and b_2 in the formulation, and constraining the permitted number of impulses (mimicking the effect of the constraint on $\min N_f$ above), we arrive at the formulation

$$(\hat{b}_1, \hat{b}_2) = \arg \min_{b_1, b_2} N_g(b_1, b_2) + \min_{b_1, b_2} N_g(b_1, b_2), \quad (8)$$

$$\text{s.t. } \#\{d_k > d_{\min}\} \leq \Pi,$$

where

$$N_g = \frac{-g(b_1, b_2)}{\partial g(b_1, b_2)/\partial b_1},$$

Π is the maximal permitted number of impulses, d_{\min} is the threshold for counting an impulse and $\#$ denotes cardinality. It should be noted that the cost function, together with the impulse number constraint, constitute a nonconvex optimization problem which admits multiple local minima.

It is however not obvious that a solution to (8) approximates (b_1^*, b_2^*) , and not some other point on γ_P . Indeed, the numerical experiments in the next section demonstrate that the estimation works well with relatively low levels of noise and a frequent sampling, but with a higher noise level, only an estimate $\hat{\gamma}_P$ of this boundary can be found. The corresponding optimization formulation then becomes

$$\bar{b}_1 = \arg \min_{b_1} N_g(b_1, \bar{b}_2) + \min_{b_1} N_g(b_1, \bar{b}_2), \quad (9)$$

$$\text{s.t. } \#\{d_k > d_{\min}\} \leq \Pi,$$

where (\bar{b}_1, \bar{b}_2) is the intersection between $\hat{\gamma}_P$ and $b_2 = \bar{b}_2$.

B. Estimation algorithms

As the optimization problems (8), (9) are non-convex, we use gridding to solve them, utilizing the finite difference over the grid points to approximate the derivative in N_g . That means that, in the low noise case, the parameter combination in the grid which minimizes N_g is used in the calculation, while in the high noise case, for each b_2 -grid point, the minimizing b_1 is used. Finally, to determine the location and weights of the impulses, all impulses below a user-defined threshold are removed and adjacent impulses are merged. The resulting procedure is summarized in Algorithm 1.

Algorithm 1 Impulse and time constant estimation

- 1: Calculate (\hat{b}_1, \hat{b}_2) from (8) (low noise) *or* solve (9) for $\bar{b}_1 = \hat{b}_1$ for a given $\bar{b}_2 = \hat{b}_2$ (high noise)
 - 2: Calculate $\hat{\theta}(\hat{b}_1, \hat{b}_2)$ from (5)
 - 3: Let $S = \{k \in \{1, \dots, K\} \mid \hat{d}_k < d_{\min}\}$
 - 4: Solve (5) with all d_k with $k \in S$ constrained to be zero
 - 5: Merge adjacent non-zero impulses according to Algorithm 1 in [7]
-

V. NUMERICAL EXPERIMENTS

The proposed estimation technique is evaluated on synthetic data consisting of the response to three impulses with additive zero-mean Gaussian measurement noise. Two Monte Carlo experiments with 100 realizations were performed; one with low noise variance (experiment A) and one with a more realistic (i.e. higher) noise level (experiment B). In the former case, a comparison is made with the implementation in [7]. The parameters of the experiments are specified in Table I, while examples of data realizations are shown in Fig. 3. The parameter values of the estimation algorithms are given in Table II.

A. Estimation from low noise-data

The ‘‘low noise’’ version of Algorithm 1 was used on synthetic data with additive measurement noise of low variance. The results are compared with the ℓ_1 -constrained estimation

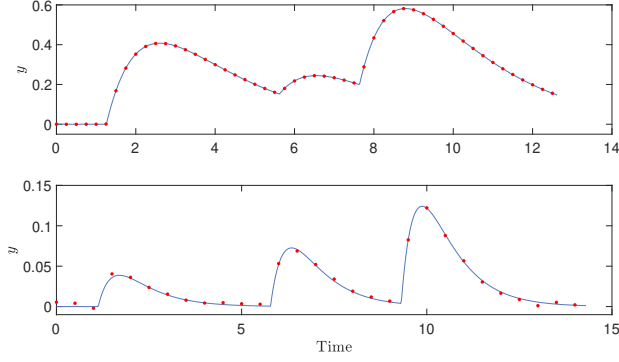


Fig. 3. Examples of sampled synthetic data with low (top) and high (bottom) levels of additive measurement noise.

TABLE I

MONTE CARLO EXPERIMENT PARAMETER DISTRIBUTIONS (LEFT) AND FIXED VALUES (RIGHT). $U_{[.,.]}$ DENOTES UNIFORM DISTRIBUTION, $\Delta\tau_i$ AND Δt_i ARE THE TIME SEPARATION BETWEEN CONSECUTIVE IMPULSES AND SAMPLES RESPECTIVELY, σ IS THE NOISE STANDARD DEVIATION AND τ_{end} IS THE TIME BETWEEN THE LAST IMPULSE AND THE END OF THE TIME HORIZON.

b_1^*	$U_{[0.4,1.4]}$		A	B
$b_2^* - b_1^*$	$U_{[0.3,1.3]}$		σ	2×10^{-4} 0.0015
d_i^*	$U_{[0.1,1]}$		Δt_i	0.25 0.5
$\Delta\tau_i$	$U_{[1,5]}$		τ_{end}	5 5

algorithm in [7], implemented with the same b_1 - b_2 -grid. To account for the regularization that is required in that method, gridding was also performed over possible values of the regularization parameter λ_{max} , and the Akaike information criterion was used to determine its value. As displayed in Table III, the current implementation performs better.

The estimated input was also evaluated. In 78% of the realizations, a correct number of impulses were estimated whereas the remaining had an average of 1.77 extra impulses caused by the noise. The impulses corresponding to the true input sequences were identified, and the resulting estimation errors are given in Table III. Both the timing and weights of the impulses are estimated with satisfactory accuracy.

B. Estimation from realistic data

Here the “high noise” version of Algorithm 1 was employed on data with a higher noise level, and less frequent sampling than the previous case, over a grid of b_2 -values. In Fig. 4, the estimate $\hat{\gamma}_P$ for one data set is displayed, together with the true parameter values and γ_P . The resulting average Euclidean distance between $\hat{\gamma}_P$ and (b_1^*, b_2^*) over all realizations is 0.0122. The curve evidently tends to be close to the true parameters, but a strategy to obtain the best estimate along this curve has not been found.

TABLE II

ESTIMATION ALGORITHM PARAMETERS. Δb IS THE DISTANCE BETWEEN THE GRID POINTS AND \bar{d} DENOTES THE MEAN IMPULSE WEIGHT.

b_1 range	$[0.5b_1^*, 0.5(b_1^* + b_2^*)]$
b_2 range	$[0.5(b_1^* + b_2^*), 1.5b_2^*]$
Δb	0.02
d_{min}	$0.05\bar{d}$
Π	$0.5K$

TABLE III

ROOT MEAN SQUARED ERRORS FOR PARAMETERS ESTIMATED USING ALGORITHM 1 (A1) AND REGULARIZED LS [7] (A2).

	A1	A2
b_1	0.0105	0.0234
b_2	0.0255	0.0582
d_i	0.0164	
τ_i	0.0745	

VI. CONCLUSIONS

A novel estimation technique for a class of continuous second-order systems with impulsive input has been presented. It builds upon previous work [7], but outperforms that method on synthetic data with low noise and also has the advantage of not requiring any data-dependent user-defined parameters. Under strong uncertainty, only an implicit relation between the plant parameters can be determined. It is hypothesized that under such circumstances, unique parameter values generally cannot be reliably estimated. A more thorough analysis of this issue, and its implications on estimations from clinical data, are possible future research directions.

APPENDIX I

PROOF OF LEMMA 1

Let $\hat{x}_i, i = 1, 2$ denote the states of the estimated system. First, consider the case of the two outputs being tangent for some $\tau > \max\{t_1, \hat{t}_1\}$, i.e. $x_2(\tau) = \hat{x}_2(\tau)$ and $\dot{x}_2(\tau) = \dot{\hat{x}}_2(\tau)$. The dynamics for x_2 and \hat{x}_2 then gives

$$\hat{x}_1(\tau) = x_1(\tau) + (\hat{b}_2 - b_2)x_2(\tau), \quad (10)$$

which is used to calculate second derivative:

$$\begin{aligned} \ddot{\hat{x}}_2(\tau) - \ddot{x}_2(\tau) &= \dot{\hat{x}}_1(\tau) - \hat{b}_2\dot{\hat{x}}_2(\tau) - \dot{x}_1(\tau) + b_2\dot{x}_2(\tau) \\ &= (b_1 - \hat{b}_1 + b_2 - \hat{b}_2)x_1(\tau) + (b_2 - \hat{b}_1)(\hat{b}_2 - b_2)x_2(\tau). \end{aligned} \quad (11)$$

Two separate cases establish the sign of this expression:

- If $\hat{b}_2 - b_2 \leq 0$ then $(b_2 - \hat{b}_1)(\hat{b}_2 - b_2) \leq 0$, so $\ddot{\hat{x}}_2(\tau) - \ddot{x}_2(\tau)$ is negative since $(b_1 - \hat{b}_1 + b_2 - \hat{b}_2) < 0$;
- If $\hat{b}_2 - b_2 > 0$, then (10) implies $\hat{x}_1(\tau) > x_1(\tau)$ and thus $\dot{\hat{x}}_1(\tau) = -\hat{b}_1\hat{x}_1(\tau) < -b_1x_1(\tau) = \dot{x}_1(\tau)$. Applying this to the first row of (11) gives $\ddot{\hat{x}}_2(\tau) - \ddot{x}_2(\tau) < 0$.

It follows that $\hat{x}_2(t) \leq x_2(t)$ in a neighborhood of τ .

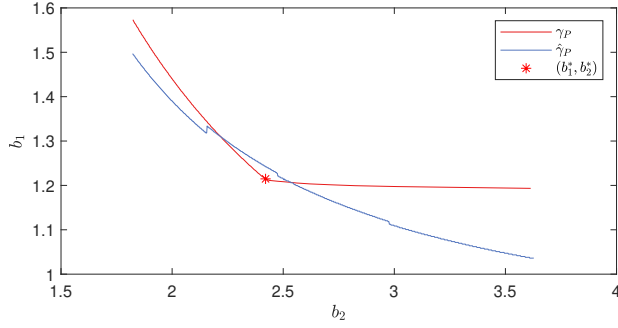


Fig. 4. The γ_P -boundary, its estimate $\hat{\gamma}_P$ generated using Algorithm 1 (with a higher grid resolution for improved visual appearance), and the true parameter values for one synthetic data realization.

Now assume that $x_2(\nu) = \hat{x}_2(\nu)$, for some $\nu \neq \tau$ and that there are no intersections between $x_2(t)$ and $\hat{x}_2(t)$ for t between τ and ν (otherwise use that intersection to define ν). Using (10) and the dynamics of the first states

$$x_1(t) = d_1 e^{-b_1(t-t_1)}, \quad \hat{x}_1(t) = \hat{d}_1 e^{-\hat{b}_1(t-\hat{t}_1)},$$

an expression for $\hat{x}_2(\nu) - x_2(\nu)$ can be calculated as

$$\begin{aligned} \hat{x}_2(\nu) - x_2(\nu) &= (b_2 - \hat{b}_2)x_2(\nu) + \hat{x}_1(\nu) - x_1(\nu) \\ &= (\hat{b}_2 - b_2)(x_2(\tau)e^{-\hat{b}_1(\nu-\tau)} - x_2(\nu)) \\ &\quad + x_1(\tau)(e^{-\hat{b}_1(\nu-\tau)} - e^{-b_1(\nu-\tau)}) \\ &= \frac{d_1}{b_1 - b_2} \left((\hat{b}_2 - b_2)e^{-b_2\nu}(e^{(\nu-\tau)(b_2-\hat{b}_1)} - 1) \right. \\ &\quad \left. + (b_1 - \hat{b}_2)e^{-b_1\nu}(e^{(\nu-\tau)(b_1-\hat{b}_1)} - 1) \right). \end{aligned}$$

Since $\hat{x}_2(\nu) - x_2(\nu) = 0$ for $\nu = \tau$, the sign is established by the derivative

$$\begin{aligned} \frac{d}{d\tau}(\hat{x}_2(\nu) - x_2(\nu)) &= \frac{d_1}{b_1 - b_2} \left((\hat{b}_2 - b_2)(\hat{b}_1 - b_2)e^{-\hat{b}_1(\nu-\tau)-b_2\tau} \right. \\ &\quad \left. + (b_1 - \hat{b}_2)(\hat{b}_1 - b_1)e^{-\hat{b}_1(\nu-\tau)-b_1\tau} \right). \end{aligned}$$

Now use $\hat{b}_2 - b_2 > b_1 - \hat{b}_1$, $\hat{b}_1 - b_2 > b_1 - \hat{b}_2$ to get

$$\begin{aligned} \frac{d}{d\tau}(\hat{x}_2(\nu) - x_2(\nu)) &> \frac{d_1}{b_1 - b_2} \left((b_1 - \hat{b}_1)(b_1 - \hat{b}_2)e^{-\hat{b}_1(\nu-\tau)-b_2\tau} \right. \\ &\quad \left. + (b_1 - \hat{b}_2)(\hat{b}_1 - b_1)e^{-\hat{b}_1(\nu-\tau)-b_1\tau} \right) \\ &= \frac{d_1}{b_1 - b_2} (b_1 - \hat{b}_1)(b_1 - \hat{b}_2)e^{-\hat{b}_1(\nu-\tau)} (e^{-\tau b_2} - e^{-\tau b_1}) > 0. \end{aligned}$$

This implies that $\hat{x}_2(\nu) - x_2(\nu)$ is positive when $\tau > \nu$, which in turn implies that $\hat{x}_2(t) > x_2(t)$ for $t > \nu$ and close to ν . Since $x_2(t)$ and $\hat{x}_2(t)$ are continuous and there are no intersections between $x_2(t)$ and $\hat{x}_2(t)$ for $\nu < t < \tau$, this is contradictory with $\hat{x}_2(t) \leq x_2(t)$ for t in a neighborhood of

τ . Since the case $\tau < \nu$ leads to a contradiction in the same way, one can conclude that if $x_2(\tau) = \hat{x}_2(\tau)$ and $\hat{x}_2(\tau) = \hat{x}_2(\tau)$, a $\nu \neq \tau$ such that $x_2(\nu) = \hat{x}_2(\nu)$ does not exist.

Now suppose that there are more than two intersections between $x_2(t)$ and $\hat{x}_2(t)$. Since $\hat{x}_2(t)$ depends linearly on \hat{d}_1 , it is then possible to reduce this weight until two of the intersections are reduced to one tangent point, while other intersections still exist (or possibly also are reduced to tangent points). But in the tangent case, there can be no other intersections between the curves, so there cannot be more than two intersections between $x_2(t)$ and $\hat{x}_2(t)$.

APPENDIX II

PROOF OF PROPOSITION 1

We only show the case $b_1 + b_2 > b_1^* + b_2^*$ and $b_1 > b_1^*$, as a similar technique can be used in the other case.

Let x_i^* , $i = 1, 2$ and x_i , $i = 1, 2$ respectively denote the states of the true and the estimated system. Consider the output of the estimated system, if it were driven by the same impulses as the true system. Since $x_2(t)$ depends monotonously on both $b_1 - b_2$ and b_2 , it then follows that $x_2(t) < x_2^*(t)$ for all $t > t_1$. Since $x_2(t)$ depends linearly on the impulse weights, the weight of the first impulse d_1 can be increased so that $x_2(t_2) = x_2^*(t_2)$. Utilizing the asymptotic behavior of the systems and Lemma 1, it can be shown that in this case $x_2(t) < x_2^*(t)$ for $t > t_2$. Now apply the same technique for the whole optimization horizon, i.e. at every t_k , increase the impulse weight (generally from zero) so that $x_2(t_{k+1}) = x_2^*(t_{k+1})$. Since this results in a solution that is optimal, and the solution is unique (see [7]), it follows that all estimated impulses are positive.

REFERENCES

- [1] J. D. Veldhuis, D. M. Keenan, and S. M. Pincus, "Motivations and methods for analyzing pulsatile hormone secretion," *Endocrine Reviews*, vol. 29, no. 7, pp. 823–864, Dec. 2008.
- [2] N. M. Davies, J. K. Takemoto, D. R. Brocks, and J. A. Yanez, "Multiple peaking phenomena in pharmacokinetic disposition," *Clinical Pharmacokinetics*, vol. 49, no. 6, pp. 351–377, 2010.
- [3] M. L. Johnson, L. Pipes, P. P. Veldhuis, L. S. Farhy, R. Nass, M. O. Thorner, and W. S. Evans, "Chapter 15 AutoDecon: A robust numerical method for the quantification of pulsatile events," in *Methods in Enzymology*. Academic Press, Jan. 2009, vol. 454, pp. 367–404.
- [4] A. Churilov, A. Medvedev, and A. Shepeljaviy, "Mathematical model of non-basal testosterone regulation in the male by pulse modulated feedback," *Automatica*, vol. 45, no. 1, pp. 78 – 85, 2009.
- [5] H. Runvik, A. Medvedev, and M. C. Kjellsson, "Impulsive feedback modeling of levodopa pharmacokinetics subject to intermittently interrupted gastric emptying," in *2020 American Control Conference (ACC)*, Jul. 2020, pp. 1323–1328.
- [6] E. Hidayat and A. Medvedev, "Parameter estimation in a pulsatile hormone secretion model," Department of Information Technology, Uppsala University, Tech. Rep. 2010-007, Mar. 2010.
- [7] P. Mattsson and A. Medvedev, "Modeling of testosterone regulation by pulse-modulated feedback: An experimental data study," *AIP Conference Proceedings*, vol. 1559, no. 1, pp. 333–342, September 2013.
- [8] H. Runvik and A. Medvedev, "Laguerre domain estimation of an input impulse train to a continuous linear time-invariant system," in *2020 59th IEEE Conference on Decision and Control (CDC)*, Dec. 2020, pp. 4622–4627.
- [9] R. Oberdieck, N. A. Diangelakis, I. Nascu, M. M. Papathanasiou, M. Sun, S. Avraamidou, and E. N. Pistikopoulos, "On multi-parametric programming and its applications in process systems engineering," *Process Systems Engineering - A Celebration in Professor Roger Sargent's 90th Year*, vol. 116, pp. 61–82, Dec. 2016.